JACS
JOURNAL OF THE AMERICAN CHEMICAL SOCIETY
pubs.acs.org/JACS
Article

Water-Hydroxyl Wetting Monolayer Predicted and Realized on a Hydrophobic Metal Surface

Meiling Xu,[¶] Qiaoxiao Zhao,[¶] Zijia Liu, Xuegao Hu, Jisong Gao, Pengyue Gao, Yiming Zhang, Yinwei Li, Dong Li, Zhicheng Gao, Kehui Wu, Lan Chen,* Changfeng Chen, Yanchao Wang,* Yanming Ma,* and Baojie Feng*

Cite This: *J. Am. Chem. Soc.* 2025, 147, 21162−21169

Read Online

ACCESS | Metrics & More | Article Recommendations | Supporting Information

ABSTRACT: Water adsorption on metal surfaces is ubiquitous in broad natural and technological settings. However, elucidating this phenomenon is often challenging due to difficulties in accurately determining the morphology and understanding the chemistry of adsorbed water networks. Here, we report a significant discovery of the water-hydroxyl (H_2O-OH) wetting monolayer, which has long been deemed possible only on hydrophilic metal surfaces, now realized on an archetypal hydrophobic metal surface, Ag(111). Ab initio structure searches predicted a hexagonal hydrogen-bonded network comprising alternating H_2O and OH units; ensuing low-energy-electron-assisted synthesis in concert with extensive characterization and computational simulation provided compelling evidence of an H_2O-OH monolayer realized on the Ag(111) surface, with remarkable stability up to near room temperature. Our finding brings new insights into the intriguing chemistry of H_2O-OH overlayers on metal surfaces, and the electron-assisted synthesis opens a unique pathway toward creating delicate molecular networks.

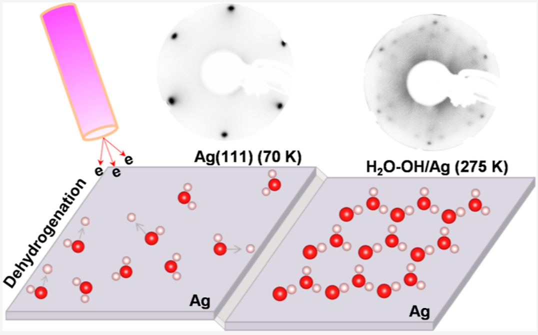

INTRODUCTION

Water adsorption on solid, especially metal, surfaces is a ubiquitous phenomenon and plays crucial roles in a wide range of physicochemical processes such as catalysis, corrosion, and electrochemistry.[1−5] Understanding water adsorption on metal surfaces is of fundamental scientific importance and carries significant practical implications, therefore having long been attracting broad interest.[6−8] The adsorption of water on active, hydrophilic metal surfaces such as Pt(111), Ru(0001), Pd(111), Cu(110), and Ni(111) is typically accompanied by spontaneous dissociation, producing hydroxyl (OH) groups, which are important and stable intermediates in the hydrogen oxidation reaction.[9] These hydrophilic metal surfaces, often taken as exemplary model substrates, allow the formation of hydrogen (H)-bonding structures of water-hydroxyl (H_2O-OH) due to thermal and electron-stimulated water dissociation.[10−20] Michaelides et al. first theoretically proposed an extended H_2O-OH overlayer structure on the Pt(111) surface.[21] Since then, a variety of mixed H_2O-OH overlayer structures have been identified on different hydrophilic metal surfaces. For example, H_2O molecules dissociate and form a hexagonal network with a 1:1 ratio of H_2O and OH arranged in a $(\sqrt{3} \times \sqrt{3})$ R30° or $p(3 \times 3)$ periodicity on hexagonal, close-packed metal surfaces.[18−20] Meanwhile, diverse structures such as extended one-dimensional $1H_2O/1OH$ chains and two-dimensional (2D) hexagonal $(2H_2O + 1OH)$ $c(2 \times 2)$ networks[22−24] were identified on open Cu(110) and Ni(110) surfaces, where the H-bonding network between H_2O and OH groups contributes to the stability of the H_2O-OH monolayer.[25] Furthermore, H_2O-OH overlayers can also form as intermediates in water formation reactions.[26]

In stark contrast to hydrophilic metal surfaces, hydrophobic metal surfaces such as Cu(111), Ag(111), and Au(111) tend to drive H_2O molecules into aggregated three-dimensional clusters rather than forming extended 2D wetting overlayers.[27−30] However, recent studies have shown that H_2O molecules can nevertheless form well-ordered, interlocked bilayer ice structures on Au(111)[31] and Au(110)[32] surfaces, which is driven by the water−water H-bonding interaction dominating over the relatively weaker water-metal interactions. These findings offer new insights into the distinct water-wetting behavior on these weakly hydrophobic surfaces.

Due to high activation barriers associated with bond breaking, producing OH groups via dissociation of water on hydrophobic surfaces is kinetically hindered.[6,8] The high temperature (well above ∼ 150 K[33]) required to dissociate water by thermal activation would lead to direct desorption of

Received: April 20, 2025
Revised: May 28, 2025
Accepted: May 29, 2025
Published: June 4, 2025

https://doi.org/10.1021/jacs.5c06679

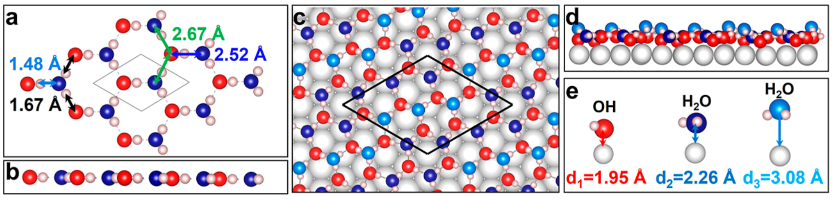

Figure 1. Structural features of the H_2O-OH monolayer. (a,b) Top and side view of the structure of the freestanding H_2O-OH monolayer. The red and dark blue spheres represent O atoms in the OH groups and H_2O molecules, respectively, while the pink spheres donate H atoms. (c,d) Top and side view of the crystal structure of $(\sqrt{7}\times\sqrt{7})$ R19.1°-$(H_2O-OH)/(4\times4)$-Ag(111). For clarity, only the Ag atoms in the top surface layer are shown. The red, dark blue, and light blue spheres represent O atoms in the OH groups, in H_2O molecules closer to the Ag surface, and in H_2O molecules farther from the Ag surface, respectively. (e) Average distances (d_1, d_2, and d_3) between the adsorbed O atoms and the Ag atoms in the top surface layer.

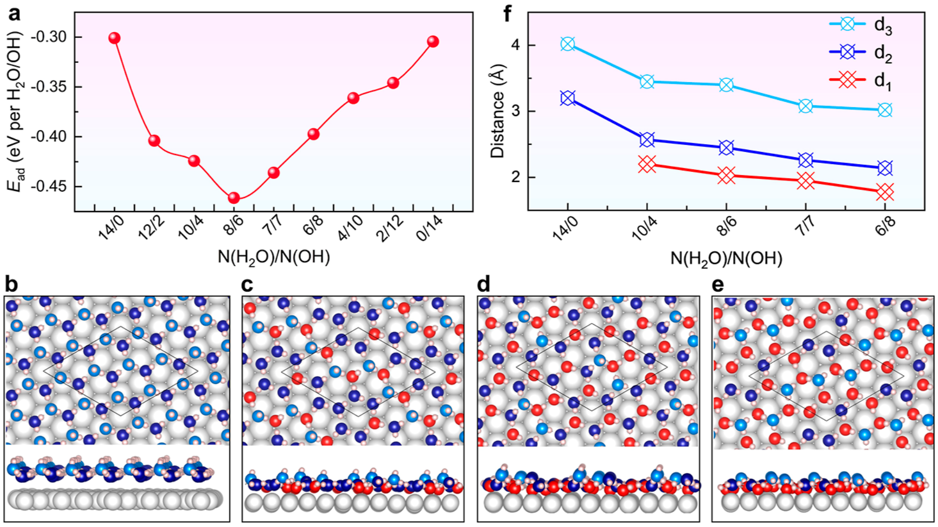

Figure 2. Adsorption energy and bonding of the H_2O-OH monolayer on Ag(111). (a) Calculated adsorption energy of the H_2O-OH monolayer with varying H_2O to OH ratios on Ag(111). (b–e) Optimized $(\sqrt{7}\times\sqrt{7})$R19.1°-14H_2O/Ag(111), $(\sqrt{7}\times\sqrt{7})$R19.1°-(10H_2O−4OH)/Ag(111), $(\sqrt{7}\times\sqrt{7})$R19.1°-(8H_2O−6OH)/Ag(111), and $(\sqrt{7}\times\sqrt{7})$R19.1°-(6H_2O−8OH)/Ag(111) structures. Red, dark blue, and light blue spheres denote O atoms in OH groups, in H_2O molecules closer to the Ag surface, and in H_2O molecules farther from the Ag surface, respectively. Additional cases are shown in Figure S2. (f) Average distances of the three types of O atoms from the Ag surface.

water from the substrate at low coverage,[34,35] instead of forming OH groups. First-principles calculations have further shown that the adsorption of $H_2O-OH-H$ overlayers on Ag(111) and Cu(111) involves significantly weaker interactions than those on hydrophilic metals such as Pt(111) and Pd(111).[36] Consequently, the formation of a H_2O-OH overlayer on hydrophobic metal surfaces has been considered infeasible in the prevailing paradigm of water adsorption on metal surfaces.

In this work, we report the discovery of a H_2O-OH wetting monolayer on a hydrophobic metal surface, Ag(111), which was first predicted via an advanced ab initio structure search and then successfully realized using a low-energy-electron-assisted (LEEA) synthesis method, which activates some H_2O molecules to dissociate into OH by electron injection at low temperatures. The synthesized H_2O-OH monolayer exhibits remarkable thermal stability up to 275 K near room temperature. This discovery sheds new light on the microscopic mechanisms that alter the morphology and chemistry of the H_2O-OH overlayer on the archetypal hydrophobic metal surface Ag(111). This mechanism is expected to be robust and applicable to additional hydrophobic metal surfaces, making what was long thought prohibitive now permissible, thereby broadening the fundamental understanding of water adsorption on structurally and chemically more diverse, technically important, and practically often encountered metal surfaces.

RESULTS AND DISCUSSION

Theoretical Prediction of the Stable H_2O-OH Monolayer on the Ag(111) Surface. We performed ab initio structure searches for freestanding H_xO_y monolayers using the CALYPSO method,[37−40] which predicted a planar H_2O-OH monolayer with layer group *cm*2*m* (No. 35),[41] with alternating H_2O molecules and OH groups interconnected via hydrogen bonds (Figure 1a,b). Note that the mixed H_2O-OH building block has been previously proposed in refs 10−20 This H_2O-OH network is analogous to the hexagonal monolayer ice structure[42,43] but with a missing hydrogen atom atop the H_2O molecule, featuring two O−O distances of 2.67 Å and 2.52 Å and distinct hydrogen bond lengths of 1.67 Å and 1.48 Å (Figure 1a). Phonon calculations confirm the dynamic stability of this freestanding H_2O-OH monolayer (Figure S1).

Adsorption of the H_2O-OH monolayer on a suitable metal substrate is expected to be favorable to its stability due to the bonding interaction between the OH groups and surface metal atoms.[8] We examined the adsorption on representative hexagonal close-packed metal surfaces, including Au(111),

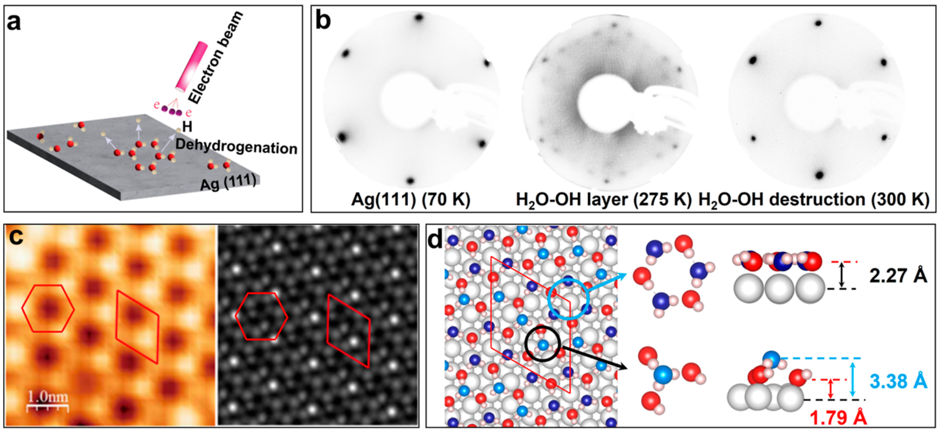

Figure 3. Synthesis and characterization of the H_2O−OH monolayer on Ag(111). (a) Schematic diagram of LEEA synthesis that induces the dissociation of H_2O into H and OH on the Ag(111) surface. (b) Measured LEED patterns: clean Ag(111) at 70 K (left), Ag(111) with H_2O coverage exposed to an electron beam of energy 120 eV for 45 s at 70 K and annealed at 275 K (middle), and then annealed at 300 K (right). (c) Measured STM image of H_2O−OH on Ag(111) (left) and simulated STM image of the $(\sqrt{7} \times \sqrt{7})$ R19.1°-7(H_2O−OH)/Ag(111) (right). The red parallelogram marks the primitive cell, and the red hexagon outlines the hexagonal bonding pattern of three bright protrusions alternating with three less bright protrusions. (d) Structure of the $(\sqrt{7} \times \sqrt{7})$ R19.1°-(H_2O−OH)/Ag monolayer (left) and the highlighted structural units underlying the bright and less bright spots in the STM image (right). The red, dark blue, and light blue spheres denote O atoms in OH groups, in H_2O molecules closer to the Ag surface, and in H_2O molecules farther from the Ag surface, respectively.

Ag(111), Cu(111), Pd(111), Pt(111), and Ru(0001). Among tested overlayer models, the $(\sqrt{7} \times \sqrt{7})$ R19.1°-(H_2O−OH)/(4 × 4)-metal structure (Figure 1c,d) matches subsequent experimental results and is adopted in the present study. The honeycomb network is well preserved on the surfaces of Ag and Au, with adsorption energies of −47 and −34 meV/atom, respectively, while the monolayer structure was disrupted on the Cu, Pd, Pt, and Ru substrates due to large lattice mismatches between the overlayer and substrates. The $(\sqrt{7} \times \sqrt{7})$ R19.1°-(H_2O−OH) monolayer has a smaller lattice mismatch of 3.10% on Ag(111) than that on the Au(111) surface (3.32%). We take Ag(111) as an exemplary template for an in-depth study of H_2O−OH adsorption on a hydrophobic metal surface.

Unlike in a freestanding H_2O−OH monolayer, the O atoms in the $(\sqrt{7} \times \sqrt{7})$-($H_2O$−OH) overlayer on Ag(111) are noncoplanar and show distinct average distances from the Ag(111) surface (Figure 1e), among which the O atoms in the OH groups have the shortest average distance of 1.95 Å, while the O atoms in the H_2O molecules fall into two categories, with the average distances of 2.26 and 3.08 Å, respectively. These results indicate that the OH groups bind more strongly than the H_2O molecules to the Ag(111) surface.

To assess the stability of the H_2O−OH overlayers with varying composition ratios, we calculated the adsorption energy as a function of the OH content within a in $(\sqrt{7} \times \sqrt{7})$ periodic model ranging from zero (14H_2O) to full (14OH). The results (Figure 2a) show that the adsorption energy for H_2O on Ag(111) is −0.3 eV/H_2O, and the formation of H_2O−OH on Ag(111) is exothermic. With rising OH content, the adsorption energy first increases, reaching the maximum (i.e., most negative) values near a 1:1H_2O to OH ratio, before decreasing with a further rise of the OH content. Therefore, the energetically optimal configuration for H_2O−OH on the Ag(111) surface contains roughly equal amounts of water and hydroxyl, forming a complete H-bonding network (Figure 1c). Higher OH ratios eventually break the complete 2D H-bonding network and lead to the dissociation of OH into H_2O and atomic O (Figure S2). Figure 2b−e shows four cases of $(\sqrt{7} \times \sqrt{7})$-($H_2O$−OH) overlayers on the (4 × 4) Ag(111) surface. It is seen that the introduction of OH groups leads to the formation of three types of O atoms, and their average distances to the Ag surface all decrease with rising OH coverage (Figure 2f), indicating enhanced interactions between the overlayer and the Ag(111) surface, thus increasing the adsorption energy (Figure 2a). Additionally, the H_2O molecules in the H_2O−OH overlayers have a smaller average distance from the Ag surface compared to those in pure H_2O adsorbed on Ag(111), suggesting that the presence of the OH groups has notably reduced the hydrophobicity of the Ag(111) surface.[44]

Synthesis of H_2O−OH Monolayer by the LEEA Method and Structural Characterization. Previous studies revealed that H_2O−OH overlayers can form on hydrophilic metal surfaces via H_2O dissociation into OH groups by thermal or electron activation.[12,16] However, the activation barrier for H_2O dissociation on hydrophobic metal surfaces is well above the desorption barrier,[8] thus inhibiting the formation of adsorbed H_2O−OH overlayers. In this work, we employed an LEEA method that enables the production of OH groups through dissociation of H_2O via electron injection at low temperatures, which was identified by our calculations, leading to successful synthesis of the H_2O−OH monolayer on an archetypal hydrophobic Ag(111) surface. Our calculations support the notion that electron injection facilitates the production of OH groups (Figure S3).

Figure 3a depicts our experimental setup for the LEEA synthesis of H_2O−OH on a Ag(111) surface. A high-quality clean Ag(111) substrate was first prepared, as verified by the sharp low-energy electron diffraction (LEED) pattern (Figures 3b and S4a). The LEED pattern deteriorated considerably and became barely visible (Figure S4b) after water coverage, which obscures the Ag(111) from LEED detection, which is an extremely surface-sensitive technique. Exposing the surface to a low-energy (120 eV) electron beam gradually brought back the 1 × 1 LEED pattern (Figure S4c), indicating the formation of a thin and uniform overlayer that once again allows a clear

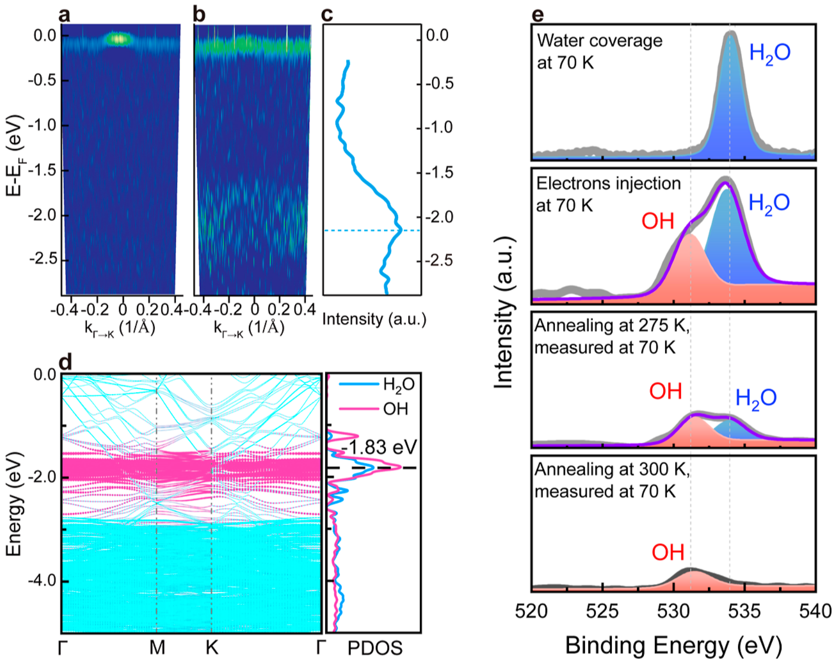

Figure 4. Measured and calculated electronic bands and XPS data for the $H_2O{-}OH$ monolayer on Ag(111). (a−c) ARPES second derivative images of the clean Ag(111) surface and the $(H_2O{-}OH)/Ag(111)$ monolayer at 70 K, along with the energy distribution curve of the latter. (d) Calculated atom-resolved electronic band structure and projected density of states (PDOS, states/eV) of $(\sqrt{7} \times \sqrt{7})$ R19.1°-$(H_2O{-}OH)/Ag(111)$. (e) XPS data of (top to bottom) H_2O on the Ag(111) surface at 70 K, after electron beam injection at 70 K, the $H_2O{-}OH$ monolayer after annealing at 275 K, and after annealing at 300 K.

imaging of the Ag(111) surface, but the overlayer is not ordered, as no new LEED spots appeared at this stage of the experiment.

The initial synthesis and characterization described above were carried out at 70 K to reduce potentially harmful thermal effects. Annealing at 220 K shows a low-quality 4 × 4 LEED pattern in alignment with the Ag(111) lattice structure (Figure S4d), indicating the thermally activated initial formation of a small-area ordered overlayer. Annealing at 260 K shows a relatively clear 4 × 4 LEED pattern (Figure S4e), representing a more extensive ordered overlayer. Subsequent annealing at 275 K brings about the clearest 4 × 4 LEED pattern (Figures 3b and S4f), indicating the formation of a large-area, long-range, well-ordered overlayer. Upon further annealing at 285 K, the 4 × 4 LEED pattern starts to fade away (Figure S4g) and disappears at 300 K (Figure 3b), indicating thermally induced structural destruction of the $H_2O{-}OH$ layer. These results show that the $H_2O{-}OH$ monolayer on Ag(111) remains stable up to near room temperature.

To characterize the synthesized $H_2O{-}OH$ overlayer on Ag(111), we performed high-resolution scanning tunneling microscopy (STM) measurements, and the obtained topographic image of the $H_2O{-}OH$ overlayer (Figure 3c, left panel) reveals a hexagonal pattern consisting of three bright protrusions alternating with three less bright protrusions. For comparison, we simulated the STM image of $(\sqrt{7} \times \sqrt{7})$ R19.1°-$(H_2O{-}OH)/Ag$ and the results (Figure 3c, right panel) are in excellent agreement with the experimental STM image. Structural analysis (Figure 3d) and integrated local density of states analysis (Figure S5) indicate that each bright protrusion (marked by a black circle) corresponds to a $H_2O(OH)_3$ unit and each less bright protrusion (marked by a blue circle) corresponds to a cyclic $OH{-}H_2O$ hexamer. The H_2O molecule in a $H_2O(OH)_3$ unit is farther from the Ag surface (3.38 Å) compared to the hexamer (2.27 Å), producing brighter spots in the STM image. A more detailed analysis has been provided in the Supplementing Information. This close agreement of the experimental and simulated STM images lends strong support to the proposed structural model of the $H_2O{-}OH$ monolayer on Ag(111). This finding is further supported by a large-area STM imaging that shows an overall submonolayer coverage of the Ag(111) surface (Figure S6) after annealing at 275 K, which provides thermal activation to equilibrate the overlayer and promote the energetically favorable monolayer $H_2O{-}OH$ on Ag(111).

Distinct Electronic Fingerprint of the $H_2O{-}OH$ Monolayer on the Ag(111) Surface. In search of a possible identifying electronic fingerprint of the $H_2O{-}OH$ monolayer on Ag(111), we probed the synthesized $(\sqrt{7} \times \sqrt{7})$ R19.1°-$(H_2O{-}OH)$ using angle-resolved photoemission spectroscopy (ARPES) (Figure 4a−c), in concert with related first-principles band-structure calculations (Figure 4d). Comparison of the measured ARPES second-derivative images of the clean Ag(111) surface (Figure 4a) and the $(\sqrt{7} \times \sqrt{7})$ R19.1°-$(H_2O{-}OH)$ monolayer (Figure 4b) reveals a set of nearly dispersionless bands distributed in an energy around ∼ 2.1 eV below the Fermi level. This flat band is also clearly observed in the energy distribution curve (Figure 4c). The corresponding calculated electronic band structure confirms the existence of flat bands in the energy range from −2.1 to −1.7 eV (Figure 4d, left panel), which produced a prominent peak in the projected density of states near −1.83 eV (Figure 4d, right panel), consistent with the ARPES measurements. In sharp contrast, the flat bands of pure water on Ag are located at much deeper energy levels, with the closest flat band positioned 4.3 eV below the Fermi level (Figure S7a), which is consistent with the ARPES measurements (Figure S7b). As a result, this agreement of the calculated and measured flat-band features serves as a distinct fingerprint in support of the proposed H_2O-OH monolayer structure on the Ag(111) surface.

Direct Detection of OH Groups in the H_2O-OH Monolayer on the Ag(111) Surface. We performed in situ X-ray photoelectron spectroscopy (XPS) measurements (Figure 4e) to probe electron injection-induced water dissociation on the Ag(111) surface under different thermal treatments. When water adsorption occurred on the clean Ag(111) surface at 70 K without electron beam irradiation, the XPS spectra of the O 1*s* core level exhibit one emission band at 533.9 eV, consistent with the binding energy of 533.4 eV of H_2O adsorption on Cu(110),[45] indicating that H_2O molecules remain intact without dissociation. Upon electron beam irradiation at 70 K, one new peak appeared at 531.3 eV, attributed to the OH groups.[44−46] At this stage, the intensity of the H_2O peak is stronger than that of the OH peak, suggesting that H_2O molecules and OH groups are not in an ordered structure, which is in agreement with the LEED results (Figure S4c). Furthermore, these findings demonstrate that H_2O molecules have dissociated to produce OH groups under electron beam irradiation at low temperatures, and the formed structure is distinct from the phases of $p(4 \times 4)$-O/Ag(111)[47−49] and H_2O-O coadsorption on metal surfaces.[50,51]

Subsequent annealing at 275 K leads to the formation of a well-ordered $(\sqrt{7} \times \sqrt{7})$ R19.1°-(H_2O-OH) overlayer. The ratio of the OH groups and H_2O molecules is nearly 1:1 in the synthesized monolayer, as evidenced by their nearly equal peak intensities. After the substrate is annealed at 300 K, the O 1*s* peak belonging to H_2O vanishes, indicating disintegration of the H_2O-OH overlayer, leaving behind some remnant OH groups on the Ag(111) surface. The XPS measurements thus provide direct evidence for the presence of dissociated OH species in the H_2O/Ag(111) system following electron beam irradiation.

Optimizing H_2O-OH Monolayer by Tuning Electron Beam Irradiation Time. The synthesis of a H_2O-OH monolayer is sensitive to electron beam exposure time, which tunes and optimizes the long-range ordered overlayer structure. Figure 5a shows the evolution of LEED patterns from the H_2O-OH/Ag(111) monolayer annealed at 275 K after different electron beam irradiation times. Short irradiation times of 15 and 30 s yield no well-defined LEED patterns beyond that of the substrate, suggesting that the brief electron beam exposure only induced dissociation of a small fraction of H_2O molecules into OH groups, which was insufficient for the formation of a well-ordered H_2O-OH network on Ag(111). After a longer, optimal electron beam exposure time of 45 s, the LEED pattern exhibits sharp diffraction spots associated with the long-range ordered $(\sqrt{7} \times \sqrt{7})$ R19.1°-(H_2O-OH) monolayer. The diffraction spots fade away (at 60 s) and then disappear (at 90 s) after further prolonged electron beam exposure, suggesting that most or all H_2O molecules have dissociated and the abundance of OH groups were unable to form well-ordered overlay structures.

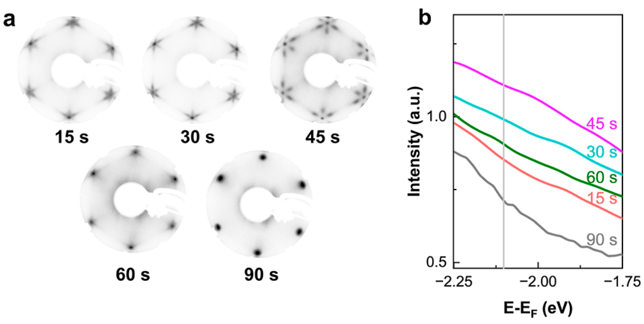

Figure 5. Effect of electron irradiation time on the long-range structural ordering of the H_2O-OH overlayer on Ag(111). (a), LEED patterns under varying electron irradiation times of the H_2O-OH monolayer on Ag(111) annealed at 275 K. (b) Corresponding energy distribution curves from ARPES measured at 70 K for the H_2O-OH monolayer on Ag(111).

Meanwhile, the energy distribution curves from flat-band regions of ARPES measurements (Figure 5b) associated with the appearance of the OH groups in the H_2O-OH network on the Ag(111) surface (Figure 4a,d) show rising intensity with the initial increase of electron irradiation time up to 45 s, which enables more extensive dissociation of H_2O molecules into OH groups, leading to increased coverage of the long-range ordered H_2O-OH network on Ag(111). Once the irradiation time exceeds the optimal 45 s, the intensity of the energy distribution curves gradually decreases, indicating damage to the well-ordered H_2O-OH monolayer. These results are consistent with the LEED patterns (Figure 5a) and calculated adsorption energies (Figure 2a), demonstrating the critical role of electron irradiation time in inducing water dissociation and tuning and optimizing the formation of the H_2O-OH monolayer on Ag(111).

Our findings suggest that the presence of OH groups can significantly reduce the intrinsic hydrophobicity of the Ag(111) surface. This transformation from a weakly interacting water−metal interface to a more hydrophilic one, driven by partial water dissociation and H-bonding network formation, provides broader insight into how surface chemistry can be tuned even on relatively inert or hydrophobic substrates. Additionally, we believe this point extends beyond Ag, suggesting that similar OH-mediated effects could play a role in modifying the water affinity on other metals or oxides typically considered hydrophobic. This has potential implications for interfacial processes, such as heterogeneous catalysis, corrosion, and electrochemical reactions.

■ CONCLUSION

Our discovery of a robust H_2O-OH wetting monolayer, which has long been considered to occur only on hydrophilic metal surfaces, represents an advancement in extending this ubiquitous phenomenon to a distinct and important class of metals, as demonstrated on the archetypal hydrophobic metal surface Ag(111). This work is built on two foundational pillars. The first is a powerful ab initio structure search method that predicted a H_2O-OH monolayer in a well-ordered, hexagonal H-bonded network; the second is an LEEA synthesis technique tailored to induce H_2O dissociation into H and OH via low-energy electron injection without destabilizing the water overlayer. Ensuing STM and ARPES measurements, along with pertinent computational simulations, provide compelling evidence supporting the formation of the $(\sqrt{7} \times \sqrt{7})$ R19.1°-(H_2O-OH)/Ag(111) monolayer, which exhibits remarkable thermal stability up to near room temperature. The H_2O-OH monolayer is expected to be achievable on broad hydrophobic metal surfaces with suitable lattice compatibility following the same protocol based on the robust low-energy electron injection mechanism. This work paves the way for exploring the wide-ranging phenomena of molecular crystal overlayer adsorption on substrates of diverse structure and chemistry characteristics.

■ METHODS

Structure Predictions and First-Principles Calculations. We performed structure searches for the freestanding H_2O−OH monolayer using the CALYPSO method.[37−40] The structural relaxations and electronic structure calculations were carried out in the framework of density functional theory (DFT),[52] as implemented in the Vienna ab initio simulation package (VASP).[53,54] The Perdew−Burke−Ernzerhof generalized gradient approximation[55] was employed to describe the exchange−correlation potential, and the projector augmented-wave potentials[56] were used to account for electron−ion interactions. In the case of the freestanding H_2O−OH monolayer, plane-wave cutoff energy of 600 eV and Monkhorst−Pack meshes[57] with a grid of 15 × 15 × 1 were adopted, ensuring energy and force convergence precisions of 10^{-6} eV and 0.01 eV/Å, respectively. For the H_2O−OH structures in the $(\sqrt{7} \times \sqrt{7})$R19.1° period on metal surfaces, the plane-wave cutoff energy of 550 eV and Monkhorst−Pack meshes[57] with a grid of 2 × 2 × 1 were adopted. These settings were chosen to ensure energy and force convergence precisions of 10^{-4} eV and 0.05 eV/Å, respectively. A six-layer slab with a 4 × 4 surface unit cell was used to model the Ag(111) surface. During structural optimization for $(\sqrt{7} \times \sqrt{7})$R19.1°-($H_2O$−OH)/(4 × 4) Ag, the lattice constants were fixed while all atomic positions were relaxed.

The adsorption energy per molecule is defined as

$$E_{\mathrm{ad}} = \frac{E_{\mathrm{tot}} - E_{\mathrm{slab}} - x\mu_{\mathrm{H_2O}} - y\left(\frac{1}{4}\mu_{\mathrm{O_2}} + \frac{1}{2}\mu_{\mathrm{H_2O}}\right)}{x + y} \tag{1}$$

where E_{tot} and E_{slab} represent the total energy of the adsorption system and the clean Ag slab, respectively. The chemical potentials $\mu_{\mathrm{H_2O}}$ and μ_{O2} refer to those of gas-phase H_2O and O_2, respectively. The parameters x and y denote the number of H_2O and OH species in the system, respectively.

Phonon calculations for the freestanding H_2O−OH monolayer were carried out using the direct supercell method implemented in the PHONOPY code[58] with a (4 × 4 × 1) supercell. The temperature-dependent effective potential method was used to determine the influence of thermal effects on the phonon dispersion relations by constructing interatomic force-constant matrices using information obtained from ab initio molecular dynamics trajectories.[59−61]

The STM images of the $(\sqrt{7} \times \sqrt{7})$ R19.1°-(H_2O−OH)/Ag(111) absorbed monolayer system were simulated using the Tersoff−Hamann approach,[62] which models an *s*-wave STM tip as follows

$$n(r, E) = \sum_{u} |\varphi_{\mu}(r)|^2 \delta(\varepsilon_u - E)$$

$$I(r, V) \propto \int_{E_{\mathrm{f}}} \mathrm{d}E_n(r, E)$$

In this method, the tunneling current, which depends on tip position r and applied voltage V, is proportional to the integrated local density of states (ILDOS) $n(r,E)$. The ILDOS is calculated from the Kohn-Sham eigenvectors, $\varphi_{\mu}(r)$, and eigenvalues, ε_u, where μ labels different states. E_{f} is the Fermi level. In our high-resolution STM measurements, we applied a voltage of −0.5 V for negative bias. This requires integrating from E_{f}−0.5 eV to E_{f} to obtain the ILDOS. We calculated the ILDOS of $(\sqrt{7} \times \sqrt{7})$ R19.1°-(H_2O−OH)/Ag(111), covering energy windows of 0.5 eV below the Fermi energy using the VASP code. The STM images were visualized using the VASP visualization tool—p4vasp software, with the tip−sample distance fixed at approximately 1.26 Å above the surface.

Sample Preparation, STM, ARPES, and XPS Experimental Measurements. Single-crystal Ag(111) was prepared by repeated cycles of Ar ion sputtering and annealing. Ultrapure H_2O (2 ppm; Alfa Aesar) was used and further purified under vacuum by freeze−pump−thaw cycles to eliminate residual impurities. H_2O molecules were dosed in situ onto the pristine Ag(111) surface held at 70 K by using a dosing tube. Electron injection was performed over the entire sample surface to ensure homogeneity. The sample was then heated to 275 K, resulting in the appearance of a 4 × 4 LEED pattern. Subsequently, the sample was cooled back to 70 K for further measurements. The successful growth of the ordered H_2O−OH monolayer was verified by using LEED and STM. STM measurements were performed in a home-built system at ∼5 K. The sample was kept at a low temperature during the transfer process. Both ARPES and XPS measurements were performed in an ultrahigh-vacuum system equipped with a hemispherical electron analyzer (SPECS PHOIBOS 150). The ARPES was conducted with a photon energy of ∼ 21 eV. XPS experiments were conducted by using an Al Kα X-ray source (SPECS XR50), and ARPES measurements were performed by using a He discharge lamp (He Iα light).

■ ASSOCIATED CONTENT

SI Supporting Information

The Supporting Information is available free of charge at https://pubs.acs.org/doi/10.1021/jacs.5c06679.

> Comparison between the experimental and simulated STM images, role of low-energy electron irradiation in water dissociation, effect of vdW interactions on the adsorption energy, phonon spectra of the freestanding H_2O−OH monolayer, crystal structures of the H_2O−OH overlayer on the Ag(111) surface with various stoichiometric ratios, mechanism of electron injection in water dissociation, LEEA synthesis of H_2O−OH monolayer on Ag(111) probed by LEED, large-area STM image of water coverage on Ag(111) annealed at 275 K, and electronic properties and ARPES measurements of pure H_2O on Ag (PDF)

■ AUTHOR INFORMATION

Corresponding Authors

Lan Chen − *Institute of Physics, Chinese Academy of Sciences, Beijing 100190, China; School of Physical Sciences, University of Chinese Academy of Sciences, Beijing 100049, China;* orcid.org/0000-0003-4426-9944; Email: lchen@iphy.ac.cn

Yanchao Wang − *Key Laboratory of Material Simulation Methods & Software of Ministry of Education, College of Physics, Jilin University, Changchun 130012, China;* orcid.org/0000-0003-4518-925X; Email: wyc@calypso.cn

Yanming Ma − *Key Laboratory of Material Simulation Methods & Software of Ministry of Education, College of Physics and International Center of Future Science, Jilin University, Changchun 130012, China;* orcid.org/0000-0003-3711-0011; Email: mym@jlu.edu.cn

Baojie Feng − *Institute of Physics, Chinese Academy of Sciences, Beijing 100190, China; School of Physical Sciences, University of Chinese Academy of Sciences, Beijing 100049, China;* orcid.org/0000-0003-2332-7949; Email: bjfeng@iphy.ac.cn

Authors

Meiling Xu − *Key Laboratory of Material Simulation Methods & Software of Ministry of Education, College of Physics, Jilin University, Changchun 130012, China; Laboratory of Quantum Functional Materials Design and Application, School of Physics and Electronic Engineering, Jiangsu Normal University, Xuzhou 221116, China;* orcid.org/0000-0001-6592-8975

Qiaoxiao Zhao − *Institute of Physics, Chinese Academy of Sciences, Beijing 100190, China; School of Physical Sciences, University of Chinese Academy of Sciences, Beijing 100049, China*

Zijia Liu − *Institute of Physics, Chinese Academy of Sciences, Beijing 100190, China; School of Physical Sciences, University of Chinese Academy of Sciences, Beijing 100049, China*

Xuegao Hu − *Institute of Physics, Chinese Academy of Sciences, Beijing 100190, China; School of Physical Sciences, University of Chinese Academy of Sciences, Beijing 100049, China*

Jisong Gao − *Institute of Physics, Chinese Academy of Sciences, Beijing 100190, China; School of Physical Sciences, University of Chinese Academy of Sciences, Beijing 100049, China*

Pengyue Gao − *Key Laboratory of Material Simulation Methods & Software of Ministry of Education, College of Physics, Jilin University, Changchun 130012, China;* orcid.org/0000-0003-1608-4934

Yiming Zhang − *Laboratory of Quantum Functional Materials Design and Application, School of Physics and Electronic Engineering, Jiangsu Normal University, Xuzhou 221116, China*

Yinwei Li − *Laboratory of Quantum Functional Materials Design and Application, School of Physics and Electronic Engineering, Jiangsu Normal University, Xuzhou 221116, China*

Dong Li − *Institute of Physics, Chinese Academy of Sciences, Beijing 100190, China; School of Physical Sciences, University of Chinese Academy of Sciences, Beijing 100049, China*

Zhicheng Gao − *Institute of Physics, Chinese Academy of Sciences, Beijing 100190, China; School of Physical Sciences, University of Chinese Academy of Sciences, Beijing 100049, China*

Kehui Wu − *Institute of Physics, Chinese Academy of Sciences, Beijing 100190, China; School of Physical Sciences, University of Chinese Academy of Sciences, Beijing 100049, China;* orcid.org/0000-0002-7698-5673

Changfeng Chen − *Department of Physics and Astronomy, University of Nevada, Las Vegas, Nevada 89154, United States*

Complete contact information is available at:
https://pubs.acs.org/10.1021/jacs.5c06679

Author Contributions

[¶]M.X. and Q.Z. contribute to this work.

Notes

The authors declare no competing financial interest.

■ ACKNOWLEDGMENTS

This work was supported by the National Natural Science Foundation of China (grant nos. T2225013, 12374010, W2411004, 12374197, 12474012, and 11904142), the National Key Research and Development Program of China (grant nos. 2022YFA1402304, 2024YFA1408400, and 2024YFA1408700), the Beijing Natural Science Foundation (grant no. JQ23001), the Strategic Priority Research Program of Chinese Academy of Sciences (grant no. XDB33030100), the CAS Project for Young Scientists in Basic Research (grant no. YSBR-047), and the Open Project of the State Key Laboratory of Superhard Materials, Jilin University (grant no. 202417). The computational resources have been provided by the High-Performance Computing Center of Jilin University and the School of Physics and Electronic Engineering of Jiangsu Normal University.

■ REFERENCES

(1) Guan, J.; Duan, Z.; Zhang, F.; Kelly, S. D.; Si, R.; Dupuis, M.; Huang, Q.; Chen, J. Q.; Tang, C.; Li, C. Water oxidation on a mononuclear manganese heterogeneous catalyst. *Nature Catalysis* **2018**, *1*, 870−877.

(2) Tian, Y.; Hong, J.; Cao, D.; You, S.; Song, Y.; Cheng, B.; Wang, Z.; Guan, D.; Liu, X.; Zhao, Z.; et al. Visualizing eigen/zundel cations and their interconversion in monolayer water on metal surfaces. *Science* **2022**, *377*, 315−319.

(3) Gonella, G.; Backus, E. H. G.; Nagata, Y.; Bonthuis, D. J.; Loche, P.; Schlaich, A.; Netz, R. R.; Kühnle, A.; McCrum, I. T.; Koper, M. T. M.; et al. Water at charged interfaces. *Nat. Rev. Chem.* **2021**, *5*, 466−485.

(4) Barry, E.; Burns, R.; Chen, W.; De Hoe, G. X.; De Oca, J. M. M.; de Pablo, J. J.; Dombrowski, J.; Elam, J. W.; Felts, A. M.; Galli, G.; et al. Advanced materials for energy-water systems: the central role of water/solid interfaces in adsorption, reactivity, and transport. *Chem. Rev.* **2021**, *121*, 9450−9501.

(5) Steinmann, S. N.; Michel, C. How to gain atomistic insights on reactions at the water/solid interface? *ACS Catal.* **2022**, *12*, 6294−6301.

(6) Hodgson, A.; Haq, S. Water adsorption and the wetting of metal surfaces. *Surf. Sci. Rep.* **2009**, *64*, 381−451.

(7) Carrasco, J.; Hodgson, A.; Michaelides, A. A molecular perspective of water at metal interfaces. *Nat. Mater.* **2012**, *11*, 667−674.

(8) Andersson, K. *Structure, Bonding and Chemistry of Water and Hydroxyl on Transition Metal Surfaces*, Ph.D. Thesis; Stockholm University, Department of Physics, 2006.

(9) Feng, Z.; Li, L.; Zheng, X.; Li, J.; Yang, Na; Ding, W.; Wei, Z. Role of hydroxyl species in hydrogen oxidation reaction: a DFT study. *J. Phys. Chem. C* **2019**, *123*, 23931−23939.

(10) Andersson, K.; Ketteler, G.; Bluhm, H.; Yamamoto, S.; Ogasawara, H.; Pettersson, L. G. M.; Salmeron, M.; Nilsson, A. Autocatalytic water dissociation on Cu(110) at near ambient conditions. *J. Am. Chem. Soc.* **2008**, *130*, 2793−2797.

(11) Feibelman, P. J. Partial dissociation of water on Ru(0001). *Science* **2002**, *295*, 99−102.

(12) Tatarkhanov, M.; Fomin, E.; Salmeron, M.; Andersson, K.; Ogasawara, H.; Pettersson, L. G. M.; Nilsson, A.; Cerdá, J. I. The structure of mixed H_2O-OH monolayer films on Ru(0001). *J. Chem. Phys.* **2008**, *129*, 154109.

(13) Zimbitas, G.; Gallagher, M. E.; Darling, G. R.; Hodgson, A. Wetting of mixed OH/H2O layers on Pt(111). *J. Chem. Phys.* **2008**, *128*, 074701.

(14) Maier, S.; Stass, I.; Cerdá, J. I.; Salmeron, M. Unveiling the mechanism of water partial dissociation on Ru(0001). *Phys. Rev. Lett.* **2014**, *112*, 126101.

(15) Schilling, M.; Behm, R. J. Partial dissociation of water on Ru(0001) at low temperatures − adsorption, structure formation and hydrogen passivation effects. *Surf. Sci.* **2018**, *674*, 32−39.

(16) Andersson, K.; Nikitin, A.; Pettersson, L. G. M.; Nilsson, A.; Ogasawara, H. Water dissociation on Ru(001): an activated process. *Phys. Rev. Lett.* **2004**, *93*, 196101.

(17) Seenivasan, H.; Tiwari, A. K. Water dissociation on Ni(100) and Ni(111): Effect of surface temperature on reactivity. *J. Chem. Phys.* **2013**, *139*, 174707.

(18) Clay, C.; Cummings, L.; Hodgson, A. Mixed water/OH structures on Pd(111). *Surf. Sci.* **2007**, *601*, 562−568.

(19) Schiros, T.; Näslund, L. Å.; Andersson, K.; Gyllenpalm, J.; Karlberg, G. S.; Odelius, M.; Ogasawara, H.; Pettersson, L. G. M.; Nilsson, A. Structure and bonding of the water-hydroxyl mixed phase on Pt(111). *J. Phys. Chem. C* **2007**, *111*, 15003−15012.

(20) Held, G.; Clay, C.; Barrett, S. D.; Haq, S.; Hodgson, A. The structure of the mixed OH+H_2O overlayer on Pt{111. *J. Chem. Phys.* **2005**, *123*, 064711.

(21) Michaelides, A.; Hu, P. A density functional theory study of hydroxyl and the intermediate in the water formation reaction on Pt. *J. Chem. Phys.* **2001**, *114*, 513−519.

(22) Forster, M.; Raval, R.; Hodgson, A.; Carrasco, J.; Michaelides, A. c(2 × 2) water-hydroxyl layer on Cu(110): a wetting layer stabilized by bjerrum defects. *Phys. Rev. Lett.* **2011**, *106*, 046103.

(23) Gerrard, N.; Mistry, K.; Darling, G. R.; Hodgson, A. Water dissociation and hydroxyl formation on Ni(110). *J. Phys. Chem. C* **2020**, *124*, 23815−23822.

(24) Forster, M.; Raval, R.; Carrasco, J.; Michaelides, A.; Hodgson, A. Water-hydroxyl phases on an open metal surface: breaking the ice rules. *Chem. Sci.* **2012**, *3*, 93−102.

(25) Clay, C.; Haq, S.; Hodgson, A. Hydrogen bonding in mixed OH+H_2O overlayers on Pt(111). *Phys. Rev. Lett.* **2004**, *92*, 046102.

(26) Michaelides, A.; Hu, P. Catalytic water formation on platinum: A first-principles study. *J. Am. Chem. Soc.* **2001**, *123*, 4235−4242.

(27) Morgenstern, K.; Nieminen, J. Intermolecular bond length of ice on Ag(111). *Phys. Rev. Lett.* **2002**, *88*, 066102.

(28) Michaelides, A.; Morgenstern, K. Ice nanoclusters at hydrophobic metal surfaces. *Nat. Mater.* **2007**, *6*, 597−601.

(29) Morgenstern, K. Scanning tunnelling microscopy investigation of water in submonolayer coverage on Ag(111). *Surf. Sci.* **2002**, *504*, 293−300.

(30) Morgenstern, K.; Rieder, K.-H. Formation of the cyclic ice hexamer via excitation of vibrational molecular modes by the scanning tunneling microscope. *J. Chem. Phys.* **2002**, *116*, 5746−5752.

(31) Ma, R.; Cao, D.; Zhu, C.; Tian, Ye; Peng, J.; Guo, J.; Chen, Ji; Li, X.-Z.; Francisco, J. S.; Zeng, X. C.; et al. Atomic imaging of the edge structure and growth of a two-dimensional hexagonal ice. *Nature* **2020**, *577*, 60−63.

(32) Yang, Pu; Zhang, C.; Sun, W.; Dong, J.; Cao, D.; Guo, J.; Jiang, Y. Robustness of bilayer hexagonal ice against surface symmetry and corrugation. *Phys. Rev. Lett.* **2022**, *129*, 046001.

(33) Andersson, K.; Gómez, A.; Glover, C.; Nordlund, D.; Öström, H.; Schiros, T.; Takahashi, O.; Ogasawara, H.; Pettersson, L. G. M.; Nilsson, A. Molecularly intact and dissociative adsorption of water on clean Cu(110): A comparison with the water/Ru (0 0 1) system. *Surf. Sci.* **2005**, *585*, L183−L189.

(34) Hinch, B. J.; Dubois, L. H. Water adsorption on Cu(111): evidence for Volmer—Weber film growth. *Chem. Phys. Lett.* **1991**, *181*, 10−15.

(35) Hinch, B. J.; Dubois, L. H. Stable and metastable phases of water adsorbed on Cu(111). *J. Chem. Phys.* **1992**, *96*, 3262−3268.

(36) Michaelides, A.; Alavi, A.; King, D. A. Insight into H_2O-ice adsorption and dissociation on metal surfaces from first-principles simulations. *Phys. Rev. B* **2004**, *69*, 113404.

(37) Wang, Y.; Lv, J.; Zhu, Li.; Ma, Y. Crystal structure prediction via particle-swarm optimization. *Phys. Rev. B* **2010**, *82*, 094116.

(38) Wang, Y.; Ma, Y. Perspective: Crystal structure prediction at high pressures. *J. Chem. Phys.* **2014**, *140*, 040901.

(39) Gao, B.; Gao, P.; Lu, S.; Lv, J.; Wang, Y.; Ma, Y. Interface structure prediction via CALYPSO method. *Sci. Bull.* **2019**, *64*, 301−309.

(40) Shao, X.; Lv, J.; Liu, P.; Shao, S.; Gao, P.; Liu, H.; Wang, Y.; Ma, Y. A symmetry-orientated divide-and-conquer method for crystal structure prediction. *J. Chem. Phys.* **2022**, *156*, 014105.

(41) J.., Fu, M.., Kuisma, A. H.., Larsen, K.., Shinohara, A.., Togo, K. S., Thygesen, Layer group classification of two-dimensional materials,arXiv. arXiv. 2401.16705 (**2024**).

(42) Chen, Ji.; Schusteritsch, G.; Pickard, C. J.; Salzmann, C. G.; Michaelides, A. Two dimensional ice from first principles: Structures and phase transitions. *Phys. Rev. Lett.* **2016**, *116*, 025501.

(43) Kapil, V.; Schran, C.; Zen, A.; Chen, Ji.; Pickard, C. J.; Michaelides, A. The first-principles phase diagram of monolayer nanoconfined water. *Nature* **2022**, *609*, 512−516.

(44) Yamamoto, S.; Andersson, K.; Bluhm, H.; Ketteler, G.; Starr, D. E.; Schiros, T.; Ogasawara, H.; Pettersson, L. G. M.; Salmeron, M.; Nilsson, A. Hydroxyl-induced wetting of metals by water at near-ambient conditions. *J. Phys. Chem. C* **2007**, *111*, 7848−7850.

(45) Spitzer, A.; Lüth, H. An XPS study of the water adsorption on Cu(110). *Surf. Sci.* **1985**, *160*, 353−361.

(46) Fisher, G. B.; Sexton, B. A. Identification of an adsorbed hydroxyl species on the Pt(111) surface. *Phys. Rev. Lett.* **1980**, *44*, 683−686.

(47) Carlisle, C. I.; King, D. A.; Bocquet, M.-L.; Cerdá, J.; Sautet, P. Imaging the surface and the interface atoms of an oxide film on Ag{111} by scanning tunneling microscopy: Experiment and theory. *Phys. Rev. Lett.* **2000**, *84*, 3899.

(48) Schnadt, J.; Michaelides, A.; Knudsen, J.; Vang, R. T.; Reuter, K.; Lægsgaard, E.; Scheffler, M.; Besenbacher, F. Revisiting the structure of the $p(4 \times 4)$ surface oxide on Ag(111). *Phys. Rev. Lett.* **2006**, *96*, 146101.

(49) Schmid, M.; Reicho, A.; Stierle, A.; Costina, I.; Klikovits, J.; Kostelnik, P.; Dubay, O.; Kresse, G.; Gustafson, J.; Lundgren, E.; et al. Structure of Ag(111)-$p(4 \times 4)$-O: No silver oxide. *Phys. Rev. Lett.* **2006**, *96*, 146102.

(50) Bange, K.; Grider, D. E.; Madey, Th E.; Sass, J. K. The surface chemistry of H_2O on clean and oxygen-covered Cu(110). *Surf. Sci.* **1984**, *137*, 38−64.

(51) Thiel, P. A.; Hoffmann, F. M.; Weinberg, W. H. Coadsorption of oxygen and water on Ru(001): Vibrational and structural properties. *Phys. Rev. Lett.* **1982**, *49*, 501.

(52) Kohn, W.; Sham, L. J. Self-consistent equations including exchange and correlation effects. *Phys. Rev.* **1965**, *140*, A1133−A1138.

(53) Kresse, G.; Hafner, J. J. P. R. B. *Ab initio* molecular dynamics for open-shell transition metals. *Phys. Rev. B* **1993**, *48*, 13115−13118.

(54) Kresse, G.; Furthmüller, J. Efficient iterative schemes for *ab initio* total-energy calculations using a plane-wave basis set. *Phys. Rev. B* **1996**, *54*, 11169−11186.

(55) Perdew, J. P.; Burke, K.; Ernzerhof, M. Generalized gradient approximation made simple. *Phys. Rev. Lett.* **1996**, *77*, 3865−3868.

(56) Blöchl, P. E. Projector augmented-wave method. *Phys. Rev. B* **1994**, *50*, 17953−17979.

(57) Monkhorst, H. J.; Pack, J. D. Special points for brillouin-zone integrations. *Phys. Rev. B* **1976**, *13*, 5188−5192.

(58) Togo, A.; Oba, F.; Tanaka, I. First-principles calculations of the ferroelastic transition between rutile-type and $CaCl_2$-type SiO_2 at high pressures. *Phys. Rev. B* **2008**, *78*, 134106.

(59) Knoop, F.; Shulumba, N.; Castellano, A.; Batista, J. P. A.; Farris, R.; Verstraete, M. J.; Heine, M.; Broido, D.; Kim, D. S.; Klarbring, J.; et al. TDEP: Temperature dependent effective potentials. *J. Open Source Softw.* **2024**, *9*, 6150.

(60) Hellman, O.; Steneteg, P.; Abrikosov, I. A.; Simak, S. I. Temperature dependent effective potential method for accurate free energy calculations of solids. *Phys. Rev. B* **2013**, *87*, 104111.

(61) Hellman, O.; Abrikosov, I. A. Temperature-dependent effective third-order interatomic force constants from first principles. *Phys. Rev. B* **2013**, *88*, 144301.

(62) Tersoff, J.; Hamann, D. R. Theory of the scanning tunneling microscope. *Phys. Rev. B* **1985**, *31*, 805−813.